Manganese 3×3 and $\sqrt{3} \times \sqrt{3}$-$R30°$ structures and structural phase transition on w-GaN(000$\bar{1}$) studied by scanning tunneling microscopy and first-principles theory

Abhijit V. Chinchore,[*] Kangkang Wang,[†] Meng Shi, Andrada Mandru, Yinghao Liu,[‡]
Muhammad Haider,[§] and Arthur R. Smith[‖]
Nanoscale and Quantum Phenomena Institute, Physics and Astronomy, Ohio University, Athens, Ohio 45701, USA

Valeria Ferrari and Maria Andrea Barral
Centro Atómico Constituyentes, GIyA, CNEA, San Martín, Buenos Aires, Argentina

Pablo Ordejón
Centre d'Investigació en Nanociència i Nanotecnologia - CIN2 (CSIC-ICN), Campus UAB, 08193 Bellaterra, Barcelona, Spain
(Received 5 January 2013; revised manuscript received 15 March 2013; published 15 April 2013)

Manganese deposited on the N-polar face of wurtzite gallium nitride [GaN (000$\bar{1}$)] results in two unique surface reconstructions, depending on the deposition temperature. At lower temperature (less than 105 °C), it is found that a metastable 3×3 structure forms. Mild annealing of this Mn 3×3 structure leads to an irreversible phase transition to a different, much more stable $\sqrt{3} \times \sqrt{3}$-$R30°$ structure which can withstand high-temperature annealing. Scanning tunneling microscopy (STM) and reflection high-energy electron diffraction data are compared with results from first-principles theoretical calculations. Theory finds a lowest-energy model for the 3×3 structure consisting of Mn trimers bonded to the Ga adlayer atoms but not with N atoms. The lowest-energy model for the more stable $\sqrt{3} \times \sqrt{3}$-$R30°$ structure involves Mn atoms substituting for Ga within the Ga adlayer and thus bonding with N atoms. Tersoff-Hamman simulations of the resulting lowest-energy structural models are found to be in very good agreement with the experimental STM images.

DOI: 10.1103/PhysRevB.87.165426 PACS number(s): 68.35.bg, 68.35.Rh, 68.37.Ef, 75.50.Pp

I. INTRODUCTION

A model spintronic semiconductor system makes use of room-temperature spin injection from a ferromagnetic (FM) material into a semiconductor (SC) material in order to achieve desirable effects such as spin-polarized transport and spin information transfer. To achieve such a model FM/SC system, there have been many efforts to investigate the deposition of FM elements onto SC surfaces. A number of papers have described, for example, the growth of iron on GaN.[1–5] Furthermore, there is great interest in general in the arrangement of atoms and atomic structures formed by depositing different elements onto the GaN(0001) surface.[6–8]

Despite the high interest in Fe, its reported triple-domain structure on the GaN(0001) surface renders it less than ideal for achieving a homogeneous magnetic thin film on GaN(0001). The possibility for a more ideal FM/SC system in GaN was first indicated in 2006 in a paper by Lu *et al.* concerning the epitaxial growth of ferromagnetic δ-MnGa onto Ga-polar wurtzite (w)-GaN(0001).[9] This system displays ideal heteroepitaxial growth with single-crystalline orientation and abrupt interface as well as the possibility to control the magnetic properties of the film by controlling the surface reconstruction during growth. Since then, MnGa/GaN has been increasingly investigated as a promising spintronic device system.[10,11]

It is therefore essential to gain an even greater understanding of Mn and MnGa layers on GaN surfaces, including the effects of Mn atoms on the surface reconstructions of w-GaN. However, there have only been a few detailed studies concerning the surface structures of Mn/w-GaN.[12,13] But, recent scanning tunneling microscopy (STM) results by Wang *et al.* have shown that a series of well-ordered $\sqrt{3} \times \sqrt{3} - R30°$ type high-density stripe phases occur on the Ga-polar w-GaN(0001) surface.[14] Wang *et al.* showed that these stripe phases are the precursors to the ferromagnetic δ-MnGa growth. Furthermore, these stripe phases comprise two-dimensional magnetic systems which have highly interesting properties of their own.

The subject of this paper is the surface structure induced by deposition of Mn onto the N-polar w-GaN(000$\bar{1}$) surface, about which even less is known. However, the intrinsic structures of the clean N-polar GaN(000$\bar{1}$) surface are well known;[15,16] these structures are distinctly different from those on the Ga-polar face.[17] Whereas the most important surface structure for Ga-polar face is the well-known pseudo-1×1, for the N-polar face it is the 1×1 Ga adlayer consisting of a single layer of Ga atoms atop the N atoms of the last GaN bilayer; this surface naturally forms a template for growth of the next GaN bilayer. Ga adatoms deposited onto the 1×1 Ga adlayer, as commonly occurring during growth, lead to formation of 3×3, 6×6, and c(6×12) adatom-on-adlayer reconstructions. These adatoms can be removed by annealing the surface, leading back to the 1×1 Ga adlayer.

The effect of Mn atoms on the N-polar Ga adlayer is an interesting subject since the Ga adlayer atoms are directly bonded to N atoms beneath via single Ga-N backbonds; by adding Mn, there exists the possibility of forming Mn-Ga-nitride structures, something which does not happen at the Ga-polar pseudo-1×1 surface. The successful formation of a smooth Mn-reconstructed GaN(000$\bar{1}$) $\sqrt{3} \times \sqrt{3}$-$R30°$ structure was reported in a reflection high-energy electron diffraction (RHEED) study in 2008.[18] Here, we report a systematic study of the structures formed by depositing Mn atoms onto the Ga adlayer. These are investigated experimentally using both RHEED and ultrahigh vacuum scanning

tunneling microscopy (UHV STM). We find well-ordered 3×3 and $\sqrt{3} \times \sqrt{3}$-$R30^\circ$ structures on this surface, one being metastable, the other being stable even to high temperatures, respectively. We also carry out first-principles calculations in order to determine suitable theoretical models. These models are presented as well as STM simulations, which are compared to the experimental data.

II. EXPERIMENTAL PROCEDURE

Samples of Mn on GaN are prepared using radio-frequency nitrogen plasma molecular beam epitaxy (rf N-plasma MBE). The MBE chamber is equipped with Ga and Mn effusion cells and a rf N-plasma source using N_2 as source gas. The base pressure of the growth chamber is below 9×10^{-11} Torr. The w-GaN(000$\bar{1}$) surface is prepared beginning with a sapphire (0001) substrate which is cleaned *ex situ* in acetone and isopropanol. It is then introduced into the UHV MBE growth chamber where it is annealed at 900 °C or higher, for 45 min or more, under N-plasma.

Next, a low-temperature GaN buffer layer is grown at a substrate temperature of 500 °C. Then, the temperature is increased to 700 °C for the main GaN layer growth. The growth is monitored using *in situ* RHEED, and samples are grown under gallium-rich conditions in order to achieve an atomically smooth surface, as indicated by a streaky RHEED pattern. The vacuum pressure is maintained at $\sim 2 \times 10^{-5}$ Torr during the growth, and a final GaN layer thickness of 2000 Å is typical.

In specific experiments to be described here, the surface is further annealed at ~700 °C in order to remove Ga adatoms and achieve the 1×1 Ga adlayer structure. This procedure requires a lot of care in order to avoid decomposition of the Ga adlayer 1×1 surface. If surface decomposition occurs, it will not be possible to achieve the 3×3 and $\sqrt{3} \times \sqrt{3}$-$R30^\circ$ reconstructions to be described here. One way to know that the surface has begun to decompose is to observe the RHEED pattern which shows a distinct *in-plane* spacing change (lattice expansion) upon loss of nitrogen by as much as 3%–4%.[19]

Once a high-quality Ga adlayer 1×1 is achieved, the surface is next exposed to a Mn dose in the range of a 0.1–0.5 ML at a sample temperature in the range 80–100 °C. The Mn dose is calibrated using a quartz crystal thickness monitor. As shown below, this leads to the formation of the Mn 3×3 reconstruction. After the Mn exposure, the surface may either be studied as is, or further prepared by annealing to temperatures up to 500 °C. In the latter case, the Mn $\sqrt{3} \times \sqrt{3}$-$R30^\circ$ reconstruction will be formed.

The prepared sample is transferred *in situ* to the STM analysis chamber which has a base pressure as low as 4×10^{-11} Torr; high-quality vacuum is essential for the STM experiments on these samples. The sample is studied using room-temperature STM, and images are recorded in constant current mode. Measurements are performed using W tips which are cleaned *ex situ* in water and isopropanol, then introduced into the UHV STM chamber and subjected to electron bombardment cleaning in order to remove oxide/hydroxide layers. After STM measurements, the sample may be transferred back to the MBE growth chamber for additional sample preparation such as annealing and/or Mn deposition.

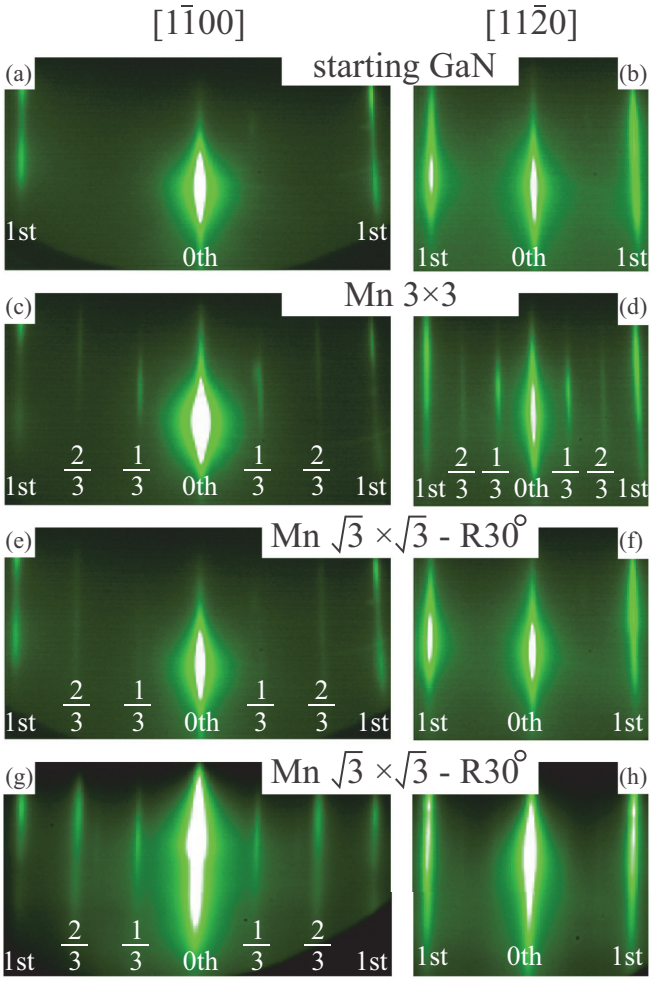

FIG. 1. (Color online) RHEED patterns. (a) and (b) GaN after growth, annealing, and cooling to room temperature; (c) and (d) after Mn deposition at 90 °C showing 3×3 with $3\times$ along both azimuths; (e) and (f) after annealing 3×3 structure surface to 250 °C showing $\sqrt{3} \times \sqrt{3}$-$R30^\circ$ structure having $3\times$ along [1$\bar{1}$00] but only $1\times$ along [11$\bar{2}$0]; (g), (h) patterns for sample with more complete $\sqrt{3} \times \sqrt{3}$-$R30^\circ$ coverage. Streak orders are labeled on the images.

III. EXPERIMENTAL RESULTS

A. RHEED observations

The starting point is to prepare a clean GaN(000$\bar{1}$) surface for subsequent Mn deposition. Shown in Figs. 1(a) and 1(b) are RHEED patterns taken along [1$\bar{1}$00] and [11$\bar{2}$0], depicting the prepared GaN surface after MBE growth and annealing, and after cooling down to room temperature. The first-order main streaks correspond to the GaN 1×1 adlayer structure. Note that the spacing between the main streaks along [1$\bar{1}$00] is $\sqrt{3}\times$ the spacing along [11$\bar{2}$0]; this is due to the threefold wurtzite lattice structure. Notably, in these RHEED patterns, there are no significant signs of $3\times$ or $6\times$ fractional streaks, suggesting the 1×1 Ga adlayer surface is relatively free of additional Ga adatoms. It is, however, difficult to completely remove all the Ga adatoms without damaging the surface due

to overannealing. In the end, the fraction of the surface having the ideal 1 × 1 Ga adlayer, and not having extra Ga adatoms nor local decomposition, is a key parameter to obtaining large areas of Mn induced 3 × 3 or $\sqrt{3} \times \sqrt{3}$-$R30^\circ$ structure.

Manganese deposition is the next step. It is found that the resulting structure is highly sensitive to the specific deposition temperature. In our 2008 paper, it was shown that deposition of Mn onto the Ga adlayer surface at 150 °C resulted in a $\sqrt{3} \times \sqrt{3}$-$R30^\circ$ surface, as indicated by a RHEED pattern having $\frac{1}{3}$- and $\frac{2}{3}$-order streaks along $[1\bar{1}00]$ but only 1× streaks along $[11\bar{2}0]$.[18] Here, we show the different set of RHEED patterns resulting from deposition of 0.3–0.5 ML of Mn at a lower temperature, 100 °C or less. As seen clearly in Figs. 1(c) and 1(d), the RHEED patterns have developed $\frac{1}{3}$- and $\frac{2}{3}$-order streaks along *both* azimuths, indicative of a 3 × 3 structure. Along both azimuths, the $\frac{1}{3}$-order streaks have at least as much intensity as the $\frac{2}{3}$-order streaks.

We note that deposition of Ga onto the Ga adlayer also results in a 3 × 3 which has previously been shown to consist of one Ga adatom per 3 × 3 unit cell, or $\frac{1}{9}$ ML Ga adatoms.[15] In contrast, the Mn 3 × 3 structure requires deposition of ∼0.3–0.5 ML of Mn to appear, which suggests that this structure contains more than one Mn atom per 3 × 3 unit cell.

Also, unlike the Ga adatom 3 × 3 reconstruction which is stable up to ∼300 °C, above which is observed a 1 × 1 structure, we find that the Mn 3 × 3 is very unstable upon annealing. After heating to only ∼115 °C, the RHEED patterns quickly transform to those corresponding to a much more stable $\sqrt{3} \times \sqrt{3}$-$R30^\circ$ structure, as seen in Figs. 1(e) and 1(f). And furthermore, unlike the Ga adatom-on-adlayer 3 × 3 structure which reforms after cooling to below ∼300 °C (reversible order-disorder transition), the Mn $\sqrt{3} \times \sqrt{3}$-$R30^\circ$ structure does not change back to the Mn 3 × 3 even after cooling to room temperature.

If the fraction of the starting surface having ideal Ga adlayer 1 × 1 structure is increased, the $\frac{1}{3}$- and $\frac{2}{3}$-order streaks along $[1\bar{1}00]$ will be brighter, corresponding to a more complete conversion of the whole surface to $\sqrt{3} \times \sqrt{3}$-$R30^\circ$ structure. This is shown in Figs. 1(g) and 1(h). From this figure, one will notice that the $\frac{2}{3}$-order streaks are brighter than the $\frac{1}{3}$-order streaks, and this feature is consistent with predictions based on the structural model for the $\sqrt{3} \times \sqrt{3}$-$R30^\circ$ reconstruction presented later in this paper.

B. Mn 3 × 3 and metastability

STM images of the Mn 3 × 3 structure reveal a regular array of atomic protrusions located on a 3 × 3 lattice, as shown in Fig. 2. The image was acquired at negative sample bias of −1.03 V and so represents the filled states of the surface. As can be seen, the 3 × 3 surface is very well ordered. A few defects are seen here and there on the surface, probably due to some foreign adsorbates. Atomic corrugation is measured along the row of ∼1.15 Å. One major protrusion is seen for each lattice site in the presented image, but due to the limited resolution, no further detail can be seen. However, as seen in the inset of Fig. 2, with a sharper tip and at a slightly more negative sample bias voltage (−1.21 V), each lattice-site protrusion can be resolved as a more complex feature consisting of several distinct lobes.

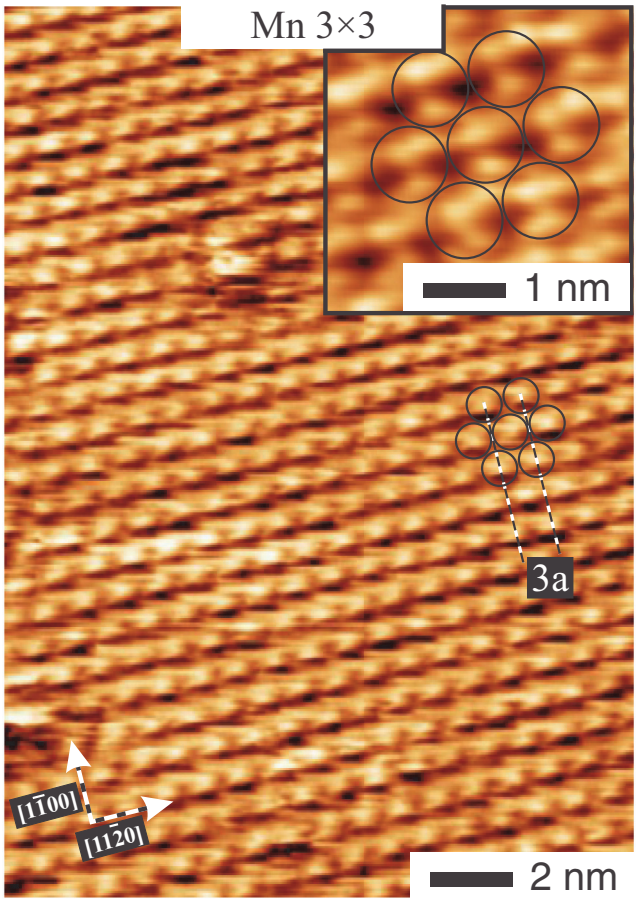

FIG. 2. (Color online) STM image of Mn 3 × 3 structure. Atomic rows are along $\langle 11\bar{2}0 \rangle$ ($V_s = -1.03$ V, $I_t = 63$ pA). Inset: Zoom-in STM image taken from the same scan area but with a sharper tip, revealing a more complex structure ($V_s = -1.21$ V, $I_t = 63$ pA).

These complex features are seen more clearly in derivative topography mode, as presented in the STM image shown in Fig. 3. Here, each 3 × 3 lattice-site protrusion is clearly resolved into a triplet of lobes. The three lobes are situated fairly symmetrically, as on the vertices of a triangle, smoothly joined in the middle, and thus forming a three-petaled flower shape. And, we observe that the orientation of the triplet is such that any line joining two lobes of the triplet is parallel to the high-symmetry $\langle 11\bar{2}0 \rangle$ surface azimuths. In the following, these triplets shall be referred to as trimers, based on the structural model. It should be noted that the image shown here was taken at the same sample region as that shown in Fig. 2, and that a tip change occurring within the same image and at the same sample bias resulted in a lower resolution image similar to that of Fig. 2. Therefore, the main difference is the tip sharpness.

The experimental data therefore suggest that the Mn 3 × 3 surface consists of a trimer structure of some type. As we show later in this paper, based on theoretical calculations, it is possible to determine that these trimer structures correspond to trimers of Mn atoms. As such, this is an unusual Mn-structured 3 × 3 surface, its intrinsic surface relative being the Ga adatom *monomer* 3 × 3, as reported by Smith *et al.*[15] Some additional features are seen in the image of Fig. 3, such as a dark/bright

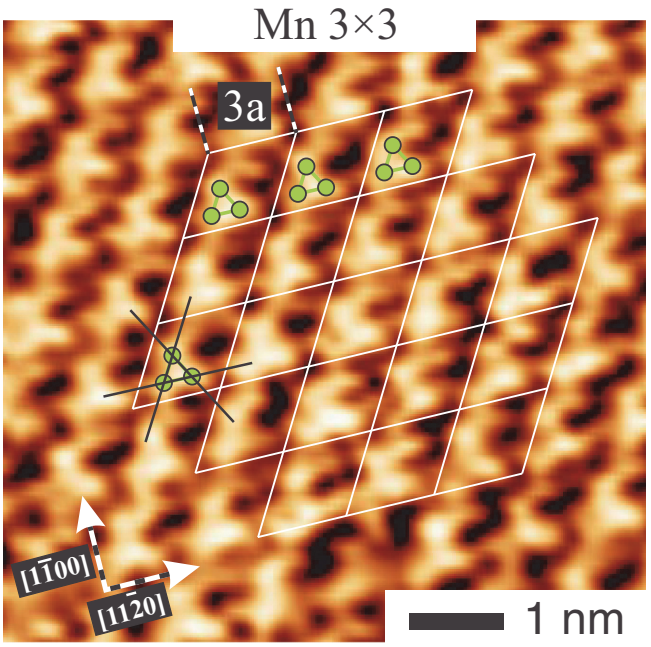

FIG. 3. (Color online) High resolution STM image (shown in derivative mode) revealing clearly a trimer structure at each lattice site ($V_s = -1.21$ V, $I_t = 63$ pA); a 3 × 3 lattice is overlaid on top of the image, along with several envisioned trimer units.

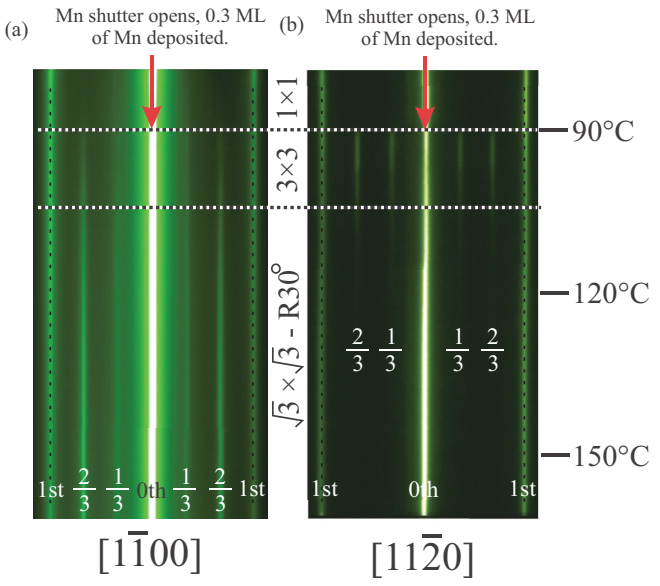

FIG. 4. (Color online) Scan mode RHEED images as a function of time and temperature (increasing from top to bottom): (a) along [1$\bar{1}$00]; (b) along [11$\bar{2}$0]. Mn is deposited, and a 3 × 3 pattern is formed; heating then begins, and the pattern begins to change towards $\sqrt{3}\times\sqrt{3}$-$R30°$. Streak orders are labeled. Black dotted lines indicate no change in RHEED spacing during the entire process. Streak spacings along [1$\bar{1}$00] and [11$\bar{2}$0] have been set equal, but should be in the ratio $\sqrt{3}$:1.

region on the other half of the unit cell (not the trimer half); only after a detailed comparison of the STM image with a theoretical model simulation will it be possible to make any specific interpretation of these features.

Shown in Figs. 4(a) and 4(b) are scan mode images along [1$\bar{1}$00] and [11$\bar{2}$0], respectively, depicting the changes occurring on the surface as a function of temperature, starting from the clean GaN surface. We clearly see the development of a 3× pattern very quickly after the Mn shutter is opened with the sample temperature during Mn deposition set at 90 °C. The intensities of the $\frac{1}{3}$- and $\frac{2}{3}$-order streaks along both azimuths at this stage are equal, which is indicative of a 3 × 3 reconstruction.

As the temperature is raised, the 3 × 3 pattern evolves into the $\sqrt{3}\times\sqrt{3}$-$R30°$ pattern. Along [1$\bar{1}$00], the pattern evolves to a stronger 3× but with unequal $\frac{1}{3}$- and $\frac{2}{3}$-order streak intensities; along [11$\bar{2}$0], the 3× pattern gradually reduces intensity and then disappears completely at close to 125 °C, at which point the pattern is fully evolved along [1$\bar{1}$00]. We can assign an irreversible phase transition temperature of ∼105 °C. Since we did not add Mn during this observed temperature transition, it suggests that the $\sqrt{3}\times\sqrt{3}$-$R30°$ and 3 × 3 structures have the same average Mn coverage. The Mn coverage is an important consideration in the theoretical modeling. As discussed more below, it is important to note that three Mn atoms in a 3 × 3 unit cell equate to the same coverage as one Mn atom in a $\sqrt{3}\times\sqrt{3}$-$R30°$ unit cell.

We also see that the dashed, vertical black lines remain centered within the first-order streaks of either azimuth from top to bottom, which tells us that the surface lattice spacing is constant throughout the entire process of Mn deposition, heating, and reconstruction phase transition. Note that over this small temperature range (90 °C–160 °C), thermal expansion is negligible.

C. Mn $\sqrt{3}\times\sqrt{3}$-$R30°$

Presented in Fig. 5(a) is a large-area STM image (acquired at −1.73 V sample bias and 96 pA tunnel current) showing two wide terraces separated by a double-bilayer w-GaN step (step height = 5.195 Å) on a 0.3-ML Mn deposited (and annealed) surface, corresponding to the RHEED patterns shown in Figs. 1(e) and 1(f). At this large-area scale, the surface appears featureless in STM except for what appear to be some random adsorbates scattered around. Otherwise, the terrace surfaces look atomically smooth, but the reconstruction can not be resolved at this scale.

Zooming in to a smaller surface region reveals that the reconstruction of the entire surface area on both terraces in Fig. 5(a) is $\sqrt{3}\times\sqrt{3}$-$R30°$. As seen in Fig. 5(b), the surface consists of a well-ordered and hexagonal array of atomic protrusions having the $\sqrt{3}\times\sqrt{3}$-$R30°$ structure with atomic spacing of $\sqrt{3}$ a. Atomic rows are aligned along ⟨1$\bar{1}$00⟩ high-symmetry directions. Every primitive unit cell of the $\sqrt{3}\times\sqrt{3}$-$R30°$ reconstruction contains not more than a single atomic protrusion, suggesting that a single Mn atom may be contained within each unit cell. Various defects/adsorbates are revealed more clearly in Fig. 5(b), some occupying an area of only about one lattice site, the bigger ones which look like adsorbates taking up around 10 lattice sites. These defects may indicate a relatively high surface reactivity.

Further zoom-in to the smaller surface region shown in Fig. 6 reveals clearly the $\sqrt{3}\times\sqrt{3}$-$R30°$ periodic structure of

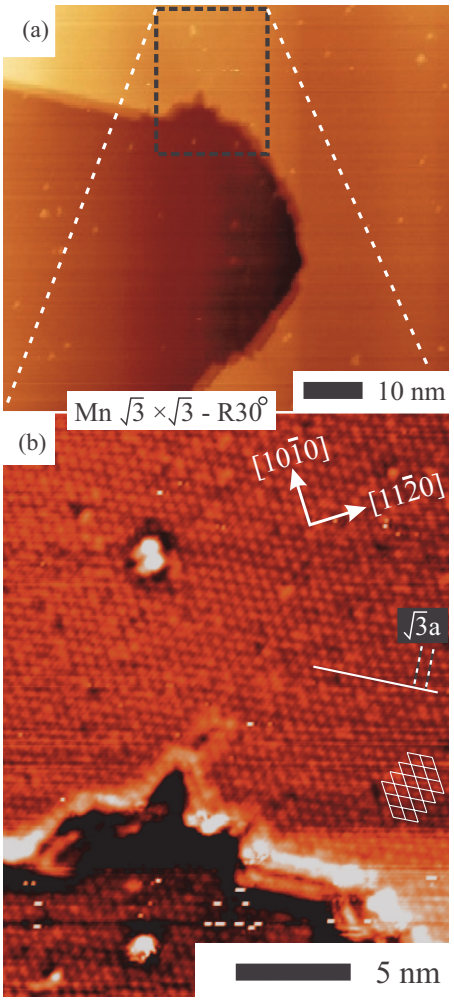

FIG. 5. (Color online) (a) Large-area STM image of $\sqrt{3} \times \sqrt{3}$-$R30^\circ$ surface. Terraces separated by a double-bilayer w-GaN(000$\bar{1}$) step; the $\sqrt{3} \times \sqrt{3}$-$R30^\circ$ structure is maintained across the step ($V_s = -2.10$ V, $I_t = 90$ pA.). (b) Zoom-in STM image revealing atomic resolution, corresponding to the dashed-boxed region in part (a) ($V_s = -1.73$ V, $I_t = 96$ pA.); a $\sqrt{3} \times \sqrt{3}$-$R30^\circ$ lattice is overlaid on the image. Image is displayed with a local area background subtraction.

protrusions having spacing of $\sqrt{3}\,a = 5.52$ Å. In this zoom-in, a phase-shift boundary is observed running diagonally across the image in the upper left corner, as marked by the jagged line. The atomic positions on either side of the phase-shift boundary form the clear hexagonal pattern; aligning dashed lines with atomic rows on either side of the boundary, and extending these lines across the boundary, it is seen that the rows on opposite sides are shifted with respect to each other by exactly one third of the $\sqrt{3} \times \sqrt{3}$-$R30^\circ$ lattice row-row spacing. This agrees with the symmetry of the $\sqrt{3} \times \sqrt{3}$-$R30^\circ$ structure since there exist two intervening atomic rows in-between consecutive rows of the $\sqrt{3} \times \sqrt{3}$-$R30^\circ$ lattice, as depicted in the inset to Fig. 6. As the $\sqrt{3} \times \sqrt{3}$-$R30^\circ$ reconstruction is forming in different regions of the surface, it may nucleate with the $\sqrt{3} \times \sqrt{3}$-$R30^\circ$ lattice sites at any of three possible unique locations. This then leads to separate domains as seen here having such one third boundary shifts.

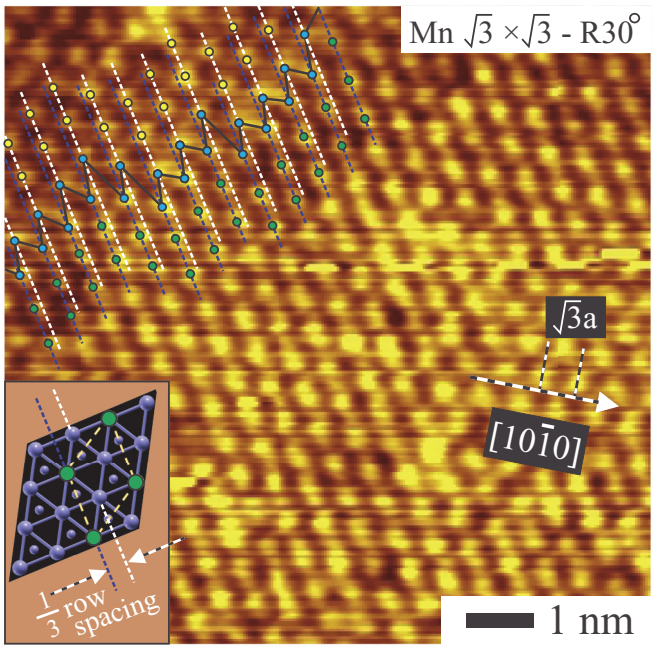

FIG. 6. (Color online) Tighter zoom-in with more atomic resolution detail for the $\sqrt{3} \times \sqrt{3}$-$R30^\circ$ surface; atomic rows on opposite sides of a phase-shift boundary (indicated by jagged black line) are shifted by one third the $\sqrt{3} \times \sqrt{3}$-$R30^\circ$ row spacing. Atomic sites on opposite sides of the boundary are indicated with yellow or green dots, interface sites indicated with blue. Inset shows detail of the reconstruction symmetry with $\sqrt{3} \times \sqrt{3}$-$R30^\circ$ lattice sites indicated in green.

One of the important aspects concerning the $\sqrt{3} \times \sqrt{3}$-$R30^\circ$ structure is that once it has formed, it is very stable and can even be observed up to temperatures as high as 750 °C. Shown in Fig. 7 is a scan mode RHEED image depicting the stability of the $\sqrt{3} \times \sqrt{3}$-$R30^\circ$ structure with respect to temperature, as seen along [1$\bar{1}$00]. The scan was acquired from a movie that was recorded as the sample temperature was being increased at a constant rate. The movie was recorded for 300 s, while the temperature of the sample rose from 25 °C to more than 750 °C. The $\sqrt{3} \times \sqrt{3}$-$R30^\circ$ pattern, as indicated most clearly by the $\frac{2}{3}$ reconstruction line, remains intact until the sample reaches ~750 °C (note that the $\frac{1}{3}$ line is too weak to see in this image). Above 750 °C, coinciding with the GaN surface decomposition temperature, the $\frac{1}{3}$- and the $\frac{2}{3}$-order streaks become spotty and eventually disappear. After surface decomposition takes place, the surface is in a disordered state, and the $\sqrt{3} \times \sqrt{3}$-$R30^\circ$ does not return even after cooling to room temperature.

Therefore, the $\sqrt{3} \times \sqrt{3}$-$R30^\circ$ structure appears to have the same stability as the GaN surface itself; such a highly stable structure suggests strong bonding between the Mn atoms and the GaN semiconductor surface. It clearly suggests that Mn atoms in the $\sqrt{3} \times \sqrt{3}$-$R30^\circ$ structure are bonding with N atoms of the GaN surface. Such a strongly bonded surface structure is certainly attractive for potential future spintronic applications requiring temperature stability. In the latter part of this paper, we show we have found theoretically that the Mn atoms are indeed bonded to the underlying N atoms in a

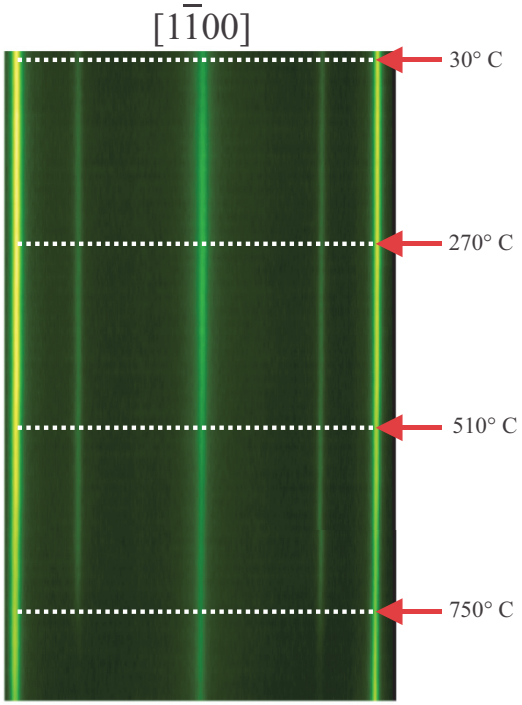

FIG. 7. (Color online) Scan mode RHEED image of $\sqrt{3} \times \sqrt{3}$-$R30^\circ$ structure as a function of time and temperature (top to bottom). Only first-order and $\frac{2}{3}$-order streaks are visible; $\frac{1}{3}$-order streaks can hardly be seen here.

structural arrangement involving a high atomic packing density within the top surface layer.

IV. THEORETICAL TECHNIQUE

In order to determine structural models of the observed surface reconstructions, we carry out density functional theory calculations using the SIESTA method.[20] The calculations are performed within the local density approximation, using the exchange-correlation potential of Ceperley-Adler[21] as parametrized by Perdew and Zunger.[22] Separable, norm-conserving pseudopotentials of the Troullier-Martins type[23] in the Kleinman-Bylander form[24] are used to describe the effect of the core electrons. Nonlinear core corrections[25] and relativistic effects are included in the pseudopotential generation. Details of the pseudopotentials and numerical atomic orbitals are given in Refs. 26 and 27. The valence wave functions are expanded in a basis set of localized atomic orbitals for every atom.

Our calculations are performed in a slab geometry with 19 alternating Ga and N layers. The bottom surface is terminated by pseudo-H atoms (artificial H atoms with ionic and electronic charge of $1.25e$), saturating the Ga dangling bonds, to emulate a bulklike behavior.[26] A vacuum of 15 Å is inserted between periodically repeated slabs. A uniform grid with an equivalent plane-wave cutoff of 300 Ry is used to perform the numerical integrations in real space. Integrations over the first Brillouin zone are replaced by discrete sums with a k-grid cutoff of 24 Å.[28] The 10 topmost layers of the slab are relaxed with the conjugate gradient method until the maximum force on each atom is under 0.04 eV/Å, while the other atoms are kept fixed at the respective positions corresponding to the bulk GaN crystal. In this paper, we are focused on the structural properties and for simplicity, we assume that the spins of all Mn atoms are aligned.

A. Theoretical model for 3 × 3 structure

In this section, we discuss the theoretical modeling of the 3×3 structure formed at low-temperature Mn deposition. Various starting structural models are proposed, one set of models considering single Mn adatoms and another set with Mn trimers, as shown in Fig. 8. The trimer models are motivated by the experimental fact that Mn coverage is not expected to change throughout the observed temperature transition (see Sec. III); therefore, the same concentration of Mn atoms as in the $\sqrt{3} \times \sqrt{3}$-$R30^\circ$ structure (i.e., $\frac{1}{3}$ ML) is expected to be maintained.

In the following, we describe the proposed models. Figure 8(a) shows the 1×1 Ga adlayer structure without Mn atoms and consists simply of one Ga per N atom. In this structure, Ga atoms are spaced by $a = 3.189$ Å, which is the surface lattice constant of GaN(000$\bar{1}$). The single/trimer Mn adatom models, T4 and H3, as presented in Figs. 8(c)–8(h), are initiated by placing one/three Mn adatoms at threefold-coordinated adatom sites; for T4, it is above the second layer Ga (which is the first GaN bilayer Ga atom), whereas for H3, it is above the hollow site of the first GaN bilayer.

We propose four different trimer Mn adatom models as shown in Figs. 8(e)–8(h). We choose these particular trimer configurations so as the three Mn adatoms of the trimer are as close as possible to each other in order to mimic the corresponding STM image (see Fig. 2). There are two available trimer models for each of the T4 and H3 configurations: two of them with a Ga atom at the center of the trimer [Figs. 8(e) and 8(f)] and two with a hollow site at the center [Figs. 8(g) and 8(h)].

In the structural models, we assume that the Mn atoms are unable to penetrate the dense Ga adlayer at the low-temperature conditions of the experiment, thus remaining on top of the surface, either in the form of trimers or single adatoms. This assumption would imply the existence of an energy barrier involved in the process of interchanging Mn and Ga atoms; the calculation of this barrier could be the subject of future studies, including molecular dynamics simulations, which are beyond the scope of this work.

To compare the energy stability of the presented models, we employ the thermodynamics formalism[29] wherein the difference in energies between structures depends linearly on the Mn chemical potential as follows:

$$\Delta E = E^{\text{model}} - E^{\text{ref}} + \Delta n_{\text{Mn}}\mu_{\text{Mn}} + \Delta n_{\text{Ga}}\mu_{\text{Ga}} + \Delta n_{\text{N}}\mu_{\text{N}}, \tag{1}$$

where E^{model} is the total energy of each of the proposed models, E^{ref} is the energy of the structure chosen as reference. Δn_{Mn}, Δn_{Ga}, and Δn_{N}, are the differences in the number of Mn, Ga, and N atoms between each model and the reference structure. μ_{Mn}, μ_{Ga}, and μ_{N} are the chemical potentials of Mn, Ga, and N, respectively. The different proposed models with 3×3 periodicity only differ in the number of Mn atoms, and therefore it is necessary to choose the range for the

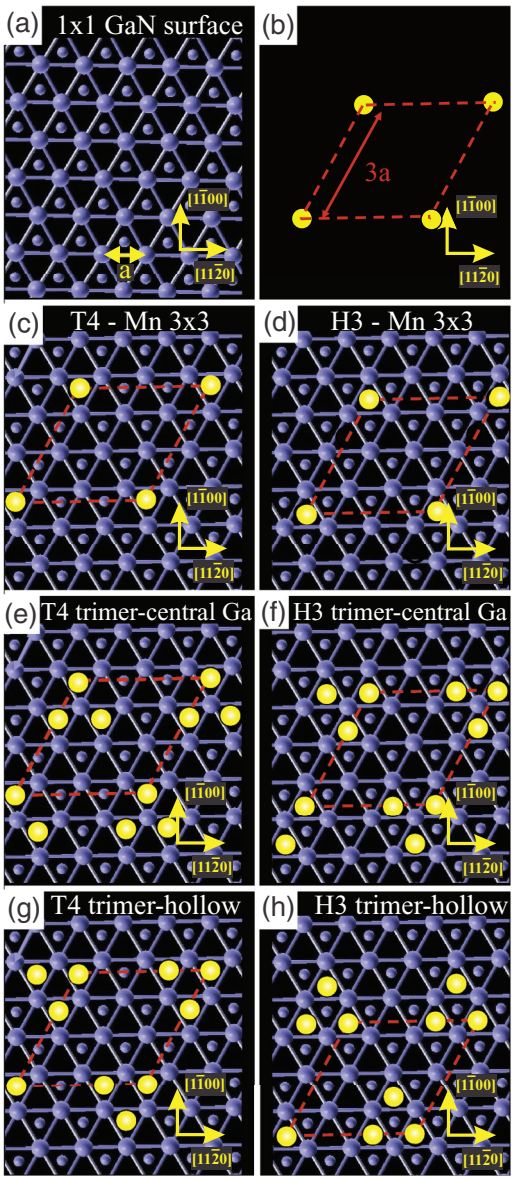

FIG. 8. (Color online) Theoretical models of the 3 × 3 structure formed by low-temperature Mn deposition. (a) Model showing Ga 1 × 1 adlayer structure without the Mn atoms; the spacing between Ga adatoms is $a = 3.189$ Å; (b) the 3 × 3 unit cell with atoms placed at 3× a spacing. In (c)–(h), the models depicted on the left correspond to single or trimer Mn adatoms located at T4 sites, while the models on the right correspond to adatoms located at H3 sites. In particular, (c) and (d) correspond to single adatoms, (e) and (f) to trimer adatoms with one Ga atom at the center of the trimer, while (g) and (h) represent trimer models with a hollow site at the center.

Mn chemical potentials to reflect the experimental conditions under which the reconstructions are formed. The upper limit for the Mn chemical potential is taken as that for metallic manganese.[30] The lower limit is evaluated by assuming thermal equilibrium of Mn either under N-rich conditions with rocksalt MnN or under Ga-rich conditions with GaMn. Those values are more stable compared to those obtained from bulk α-Mn by 0.86 eV and 0.4 eV/Mn, respectively.[31]

In Fig. 9, we show the energy plots for the different models. From this figure, it turns out that the trimer models without

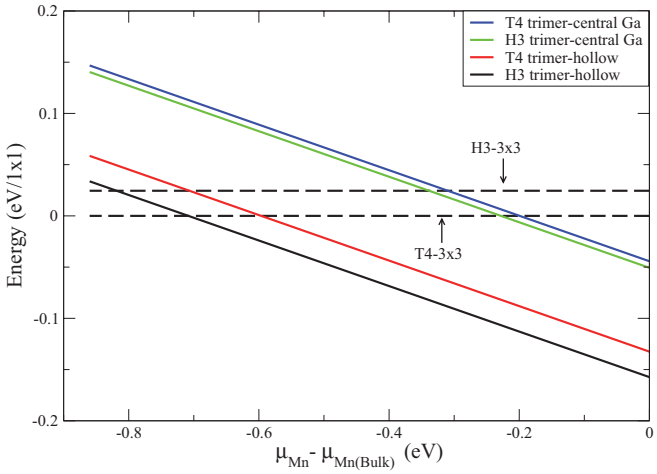

FIG. 9. (Color online) Energy plots for the various 3 × 3 models depicted in Fig. 8. The dashed lines correspond to the 3 × 3 structure with single Mn adatoms. The solid colored lines correspond to the 3 × 3 models with trimer Mn adatoms. In the trimer models, both T4 and H3 can have the trimer either with a central Ga atom or without it (hollow), as indicated in the legend. The reference structure is the T4 single Mn model.

central Ga are the structures favored by energetics. Of these two, the H3 trimer hollow is the most energetically favorable structure over the largest range of Mn chemical potential, corresponding to the starting structure of Fig. 8(h). This structure relaxes as shown in Fig. 10. The top-view image shown in Fig. 10(a) reveals that the Mn trimer clearly pushes the three neighboring Ga adlayer atoms (first three, adjacent to trimer edges) outward away from the center of the trimer, exposing the N atoms below. The second three Ga atoms neighboring the Mn trimer (at the trimer vertices) are less affected by this push. The three Ga atoms not neighboring the Mn trimer are deflected more due to the fact that they are neighbors of the first three deflected Ga's; this is observed as a slight shift of these Ga atoms off a straight line drawn along $\langle 11\bar{2}0 \rangle$ directions, making them appear to be in a staggered line. This outward push is observed in the side-view image [Fig. 10(b)] as a bond rotation (or canting) of the Ga-N bonds away from the [000$\bar{1}$] surface normal. As such, the Mn atoms

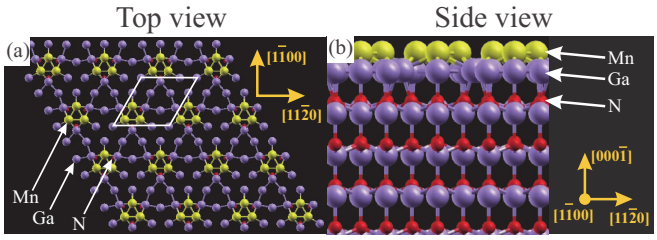

FIG. 10. (Color online) The energetically stable model for the H3 Mn trimer 3 × 3, after relaxation. (a) Top-view image, revealing the various lateral displacements of Ga atom positions due to the Mn trimer; (b) side-view image, showing the bond canting of Ga-N bonds away from the [000$\bar{1}$] surface normal direction, enabling Mn to settle into the surface. Mn atoms are bonded only with Ga atoms and not with N.

are allowed to settle into the surface, closer to the Ga adlayer due to the *in-plane* lateral displacement of the Ga atoms.

In the side-view image of Fig. 10(b), aside from the Ga-N bond canting away from the surface normal created by the Mn trimer, the surface just consists of the Mn trimer layer as the top layer, followed by the Ga adlayer which is bonded to the N atoms in the third layer (part of the first GaN bilayer). From that point going deeper into the surface, the normal sequence of GaN bilayers is observed. It is a key point to notice that in the H3 Mn trimer model, Mn atoms are only in ad-trimer positions bonding with Ga, and never with N. This is a distinguishing characteristic, and it is crucial for understanding the irreversible $3 \times 3 \rightarrow \sqrt{3} \times \sqrt{3}$-$R30^\circ$ phase transition which comes by slight heating.

It is interesting to note that the trimer structures are energetically preferred over the single ones, in agreement with a Mn-Mn clustering behavior found in Mn-doped bulk GaN calculations.[31] In the trimer structures, the Mn-Mn distance changes from 3.19 Å to about 2.7 Å as a result of atomic relaxation, getting closer to the Mn-Mn distance in bulk α-Mn.[31]

The simulation of the STM image [done within the Tersoff-Hamman (T-H) approximation[32]] of the stable H3 trimer-hollow model compared to the experimental data is presented in Fig. 11. The occupied-states STM image and T-H simulated image are displayed together with overlays of the H3 trimer-hollow model structure in Figs. 11(a) and 11(b), respectively. The T-H simulation predominantly reveals that the Mn trimer appears as a bright lobe in occupied states. This lobe is roundish in shape at the calculated energy, but also has a slight triangular appearance which may be partly due to the three Ga atoms neighboring, and bonded off the vertices of, the Mn trimer. The three Ga atoms bonded off the edges of the trimer hardly appear at all in occupied states. On the other hand, the three Ga atoms having no Mn neighbors do stand out in the simulation as brighter spots against a darker background (but much weaker than the Mn trimer lobes).

Comparing this H3 trimer-hollow T-H simulation with the experimental STM image [as shown in Fig. 11(a)], we find a very good agreement. In fact, the trimer atoms are more clearly resolved in the experimental image as compared to the simulation. We note that the orientation of the trimers

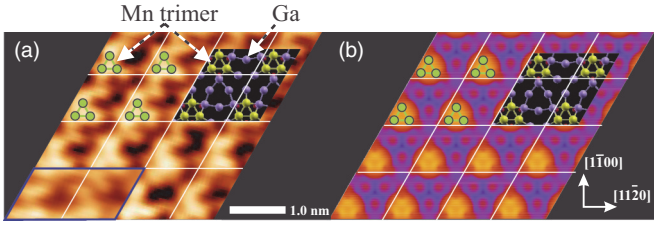

FIG. 11. (Color online) STM image (left) and T-H simulation (right) of the stable H3 Mn trimer-hollow structure. (a) Occupied-states STM image ($V_s = -1.21$ V, $I_t = 63$ pA), with an overlay of the relaxed H3 trimer-hollow model. Bright protrusions correspond to Mn trimers; (b) occupied-states T-H simulated image with an overlay of the H3 trimer-hollow model. The Mn trimers correspond to the bright lobes. STM image in (a) shown in derivative mode, except for lower left two unit cells which are shown in topography mode (blue boxed region).

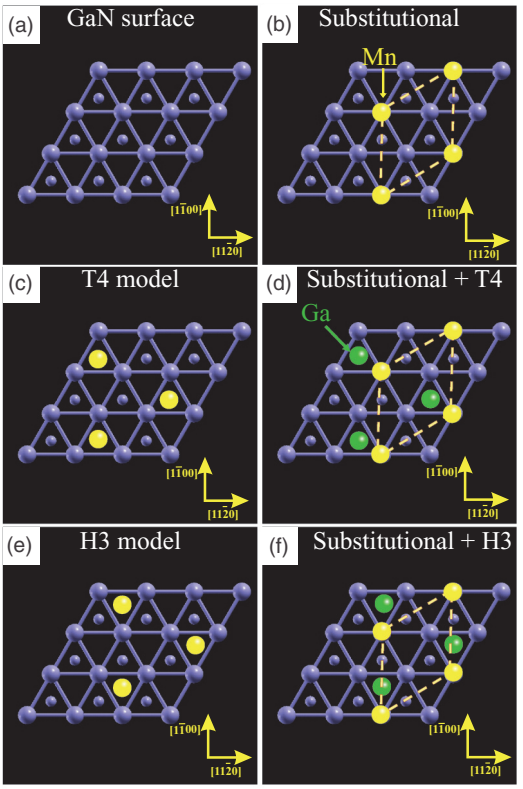

FIG. 12. (Color online) Structural models considered for the $\sqrt{3} \times \sqrt{3}$-$R30^\circ$. (a) Ga 1×1 adlayer structure without Mn atoms. (b), (c), and (e) depict structural models with Mn atoms in the substitutional, T4 adatom, and H3 adatom sites, respectively. (d) and (f) correspond to the substitutional + T4 and substitutional + H3 models, respectively.

is the same for both experiment and simulation, reflecting the correct structure of the model. The bright three-lobed protrusions seen in the STM image (occupied states), and occupying about one half of the 3×3 unit cell, can thus be identified as corresponding to the Mn trimers.

B. Theoretical model for $\sqrt{3} \times \sqrt{3}$-$R30^\circ$ structure

Theoretical calculations are also performed to determine the lowest-energy structural model for the $\sqrt{3} \times \sqrt{3}$-$R30^\circ$ structure. The starting models include substitutional, T4, and H3 adatom and also substitutional + T4 (or H3) adatom models. We explain each structure in the following. The Ga adlayer 1×1 is reproduced in Fig. 12(a). From this structure, the starting $\sqrt{3} \times \sqrt{3}$-$R30^\circ$ substitutional model is formed by replacing Ga with Mn at all the $\sqrt{3} \times \sqrt{3}$-$R30^\circ$ sites which are located at sites $\sqrt{3} \times a$ along the $\langle 1\bar{1}00 \rangle$ directions, as shown in Fig. 12(b). The T4 model consists of Mn located directly above second-layer Ga, while the H3 one consists of Mn located above hollow sites of the first GaN bilayer as seen in Figs. 12(c) and 12(e), respectively. Two additional substitutional models are considered, namely, the substitutional + T4 model and the substitutional + H3 model, whose initial structures are shown in Figs. 12(d) and 12(f), respectively. These structures are obtained by interchanging the Mn adatom in the original T4 (or H3) model and a Ga atom from the Ga adlayer. Note that the substitutional model has one Ga atom less than all the other

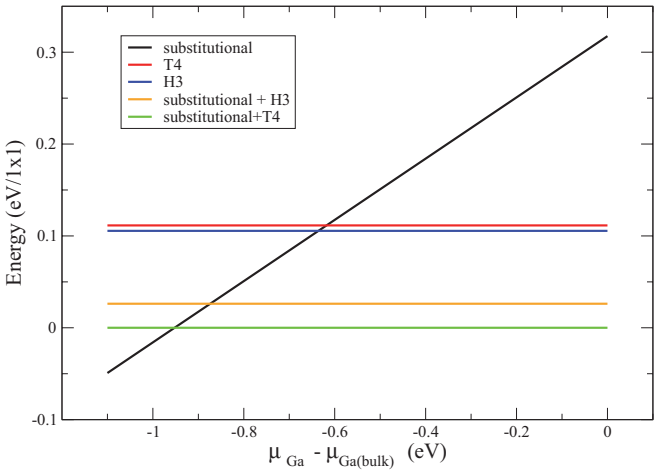

FIG. 13. (Color online) Energy plots versus Ga chemical potential for the theoretical models considered for the $\sqrt{3} \times \sqrt{3}$-$R30^\circ$ as shown in Fig 12. The substitutional + T4 model is found to be lowest in energy over most of the range of Ga chemical potential considered, and it is chosen as the reference structure.

proposed structures and, therefore, for evaluating the relative stability, a suitable range for the Ga chemical potential should be chosen. We take as the upper limit for the Ga chemical potential the one for bulk metallic Ga, while for the lower limit, the Ga chemical potential in bulk GaN.[15]

As can be seen from the energy diagram in Fig. 13, the substitutional models are always the ones which lie lower in energy and, in particular, the substitutional + T4 model is the preferred one over most of the range of Ga chemical potential. The T4 and H3 adatom models are much higher in energy.

The final relaxed substitutional + T4 model (shown in Fig. 14) turns out to look quite different as compared to the starting point model. Namely, on allowing structural relaxation to converge, significant atomic displacements are observed. The top view of the model in Fig. 14(a) shows that all surface Ga atoms have shifted, resulting in a effective 30° rotation of the Ga adlayer sublattice. From the side-view model shown in Fig. 14(b), this lateral shift is observed as Ga-N bonds tilting away from the [000$\bar{1}$] normal direction, leading to staggered

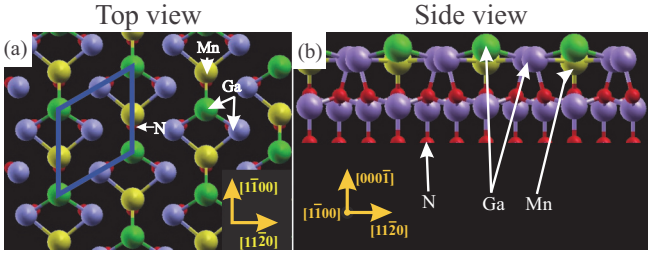

FIG. 14. (Color online) Top and side views of the final relaxed substitutional + T4 model for the $\sqrt{3} \times \sqrt{3}$-$R30^\circ$. The color coding of the atoms is the same as Fig. 10. (a) Top view of substitutional + T4 structure, in which atomic displacement results in an effective 30° rotation of the Ga adlayer sublattice; (b) side-view model revealing clearly the bonding between Mn and N as well as the Ga-N bonds tilting away from [000$\bar{1}$]. The Mn-N bonds are also tilted away from [000$\bar{1}$], but in the direction of [1$\bar{1}$00].

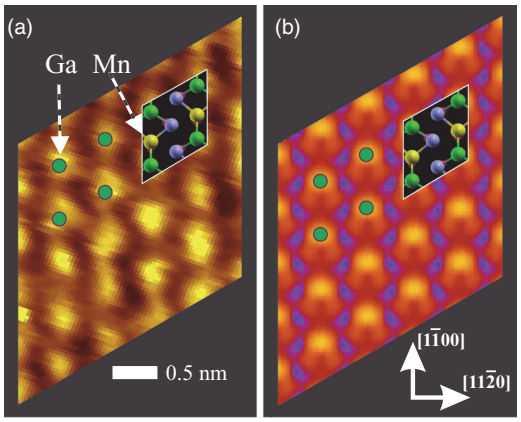

FIG. 15. (Color online) Comparison of occupied-states STM image ($V_s = -1.73$ V, $I_t = 96$ pA.) with T-H occupied-states simulation for the $\sqrt{3} \times \sqrt{3}$-$R30^\circ$. The substitutional + T4 model structure is overlaid onto both the STM image and the T-H simulation, showing clearly that Mn atoms correspond to depression sites in the image. Whereas, the protrusions seen in the occupied-states STM image correspond to the locations of the Ga adatoms.

Ga-N bond angles when sighting along [1$\bar{1}$00]. The Mn atom bonded to N is also tilted away from the [000$\bar{1}$] normal direction by ~25°, but in the direction of [1$\bar{1}$00]. Finally, the extra Ga atom ends up sinking fairly low into the surface, bonded only to two Ga atoms and one Mn atom, but not to the nitrogen.

The resulting $\sqrt{3} \times \sqrt{3}$-$R30^\circ$ substitutional + T4 model can also be viewed as consisting of chains of $MnGa_3$ units running along [1$\bar{1}$00] and having two Ga and one Mn bonded to N atoms beneath + 1 Ga adatom, as suggested in Fig. 14(a). Regarding the atomic coverage, it should be noted that all three Ga per $\sqrt{3} \times \sqrt{3}$-$R30^\circ$ unit cell are retained in the model, so therefore the atomic coverage is three Ga + 1 Mn per $\sqrt{3} \times \sqrt{3}$-$R30^\circ$ cell = $\frac{4}{3}$ ML, higher than the clean Ga adlayer surface, which is due to the sublattice rotations and resultant increased packing density.

It is interesting that if one just considers the Mn and Ga atom layer, a nearly identical (0001)-projected structural model was also found for the case of a $\sqrt{3} \times \sqrt{3}$-$R30^\circ$ structure occurring on the Ga-polar face [w-GaN(0001)].[14] In the Ga-polar case, however, the rotated and $\frac{4}{3}$-ML coverage $\sqrt{3} \times \sqrt{3}$-$R30^\circ$ structure occurs at the first (top) layer of the well-known Ga double layer. The second layer remains a pure Ga layer in a bulklike and nonrotated arrangement. In that case, the Mn and Ga atoms in the first layer clearly do not bond with N atoms, and instead are only bonded to the second-layer Ga atoms. With this distinction, it is amazing to see that this type of high-density $\frac{4}{3}$-ML $\sqrt{3} \times \sqrt{3}$-$R30^\circ$ structural model is still favored on the (000$\bar{1}$) surface since it requires significant bond tiltings as observed in Fig. 14(b).

STM simulations have been carried out under constant current conditions, in the T-H approximation, to compare the substitutional + T4 model directly to the STM images, as seen in Fig. 15. The T-H simulation corresponds to the occupied states. The substitutional + T4 model structure is overlaid on the simulation where it is seen that Mn atoms correspond to depression sites in the image. Given that the model structure

is not threefold symmetric, it can also be seen that the chains of $MnGa_3$ units run along the $[1\bar{1}00]$ direction creating as well valleys running along the same direction and not along 120°-rotated directions.

The T-H simulation [Fig. 15(b)] is directly compared to the zoom-in STM image [Fig. 15(a)]. The STM image is also overlaid with the structural model in order to make a direct comparison. Based on the T-H simulation, we may thus interpret that the protrusions seen in this occupied-states image correspond to the locations of the Ga adatoms of the substitutional + T4 structure. Furthermore, we also observe that the valleys created by the non-threefold-symmetric structure are suggested in this particular image. Therefore, based on the very good agreement between the experimental and theoretical data, it is concluded that the substitutional + T4 model is a reasonable one for this reconstruction.

C. Theoretical study as a function of the Mn coverage at low temperatures

As described in previous sections, at low temperatures only the 3×3 periodicity appears in the experiments, even if the Mn dose is increased. To study the influence of the effect of different Mn coverage, we also consider theoretical models with other possible periodicities. As a whole, we have 3×3, $\sqrt{3} \times \sqrt{3}$-$R30°$, 2×1, and 1×1, which correspond to Mn coverages of $\frac{1}{9}$, $\frac{1}{3}$, $\frac{1}{2}$, and 1, respectively. Moreover, the trimer structure in the 3×3 periodicity presents an alternative model to study the same coverage as the $\sqrt{3} \times \sqrt{3}$-$R30°$ structure with a single Mn adatom. The studied models are all under the assumption that the Mn atoms are deposited as adatoms, as previously assumed for low temperatures. In all cases, the T4 and H3 adatom configurations were considered.

In Fig. 16, we show the relative stability of the different periodicities for the range of Mn chemical potentials considered previously. It can be seen that in most of the range of Mn chemical potential, the two structures that prevail are the $\sqrt{3} \times \sqrt{3}$-$R30°$ and the trimer 3×3. We note that both

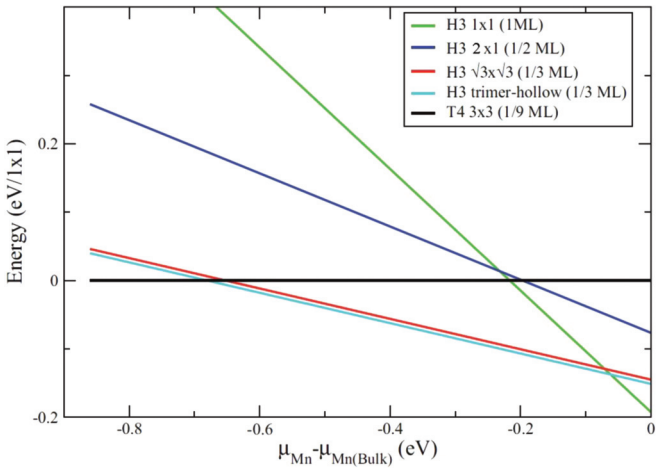

FIG. 16. (Color online) Energy plots for structures with different periodicity and Mn coverage. For all cases, the T4 and H3 models are considered, but only the lowest-energy one is pictured. In the legend, the models are stated and the Mn coverage is indicated between parentheses. The reference structure is the T4 single Mn model.

structures have the $\frac{1}{3}$-ML coverage, with the trimer being the most stable one, in agreement with the periodicity observed in the experiments at low temperatures.

D. Possible scenario for the 3×3 to $\sqrt{3} \times \sqrt{3}$-$R30°$ transition

In this section, we briefly discuss a plausible scenario to understand the 3×3 to $\sqrt{3} \times \sqrt{3}$-$R30°$ phase transition. The initial low-temperature structure is the Mn trimer with 3×3 periodicity in the H3 model, as described in Sec. IV A. When the temperature increases above 105 °C, the system would begin to surpass the energy barrier suggested by the experiments, thus breaking up the Mn-Mn bonds present in the trimers. The Mn adatoms would then have enough energy to diffuse across the surface and interchange with Ga atoms, ending up in the structure with $\sqrt{3} \times \sqrt{3}$-$R30°$ periodicity as in the substitutional + T4 model discussed in Sec. IV B. It is important to note that the total energy for this final structure is lower by about 100 meV (per 1×1 unit cell) compared to the initial 3×3 model with the Mn trimers as adatoms, which explains why the temperature transition is irreversible.

V. SUMMARY

Submonolayer Mn deposition onto the N-polar gallium nitride$(000\bar{1})$ surface is shown to lead to two different structures depending on the substrate temperature. At very low deposition temperature, a metastable 3×3 structure is formed, whereas at higher deposition temperatures or after mild annealing of the 3×3, a much more stable $\sqrt{3} \times \sqrt{3}$-$R30°$ structure forms. The transformation from 3×3 to $\sqrt{3} \times \sqrt{3}$-$R30°$ upon mild annealing is irreversible, and it is concluded based on the experimental data that the 3×3 is a metastable structure, whereas the $\sqrt{3} \times \sqrt{3}$-$R30°$ structure is highly stable even up to high temperatures. First-principles calculations find lowest-energy structural models for both the metastable 3×3 as well as the stable $\sqrt{3} \times \sqrt{3}$-$R30°$, namely, an H3 Mn trimer model for the 3×3 and a substitutional + T4 model for the $\sqrt{3} \times \sqrt{3}$-$R30°$. Very good agreement is found between T-H simulations of these models and the actual STM images. It may be concluded that the metastability of the 3×3 is due to the fact that Mn are bonded only to Ga atoms, while only a small activation barrier prevents this structure from transforming into the $\sqrt{3} \times \sqrt{3}$-$R30°$, which can be overcome through heating. Since both structures have the same surface coverage on average, therefore, the 3×3 structure transforms directly into the $\sqrt{3} \times \sqrt{3}$-$R30°$, after which point the Mn atoms become bonded to subsurface N atoms. It is also amazing that the arrangement of Mn and Ga atoms in the $\sqrt{3} \times \sqrt{3}$-$R30°$ structure which forms on N-polar GaN 1×1 is so similar to the corresponding arrangement which occurs on the Ga-polar pseudo-1×1, namely, a higher density, rotated structure in comparison with the underlying atoms: N atoms in the N-polar case and Ga atoms in the Ga-polar case. The reason for this striking similarity can only be guessed at, but it is possible that the stability of the MnGa structure is the driving force behind the observed arrangement in both cases.

ACKNOWLEDGMENTS

Research supported by the US Department of Energy, Office of Basic Energy Sciences, Division of Materials Sciences and Engineering under Award No. DE-FG02-06ER46317 (STM studies of nanoscale spintronic nitride systems) and by the National Science Foundation under Award No. 0730257 (advancing nanospintronics through international collaboration). V.F. and M.A.B. would like to acknowledge support from CONICET (PIP0038) and ANPCyT (PICT1857) as well as the Ohio Supercomputing Center for computer time. P.O. was supported by Spanish MICINN (FIS2009-12721-C04-01, FIS2012-37549-C05-02 and CSD2007-00050). We thank N. Sandler for helpful discussions during the project and for fostering the present collaboration. The authors also thank WSxM developers for use of the WSxM image processing software.[33]

*Current address: Intel Corporation, Hillsboro, OR 97123.

†Current address: Seagate Technologies, 47010 Kato Rd., Fremont, CA 94538.

‡Current address: University of Oregon, 1254 Franklin Blvd., Eugene, OR 97403.

§Current address: King Fahd University, P. O. Box 1821, Dhahran, 31261, Saudi Arabia.

‖Corresponding author: smitha2@ohio.edu

[1] R. Calarco, R. Meijers, N. Kaluza, V. A. Guzenko, N. Thillosen, T. Schapers, H. Luth, M. Fonin, S. Krzyk, R. Ghadimi, B. Beschoten, and G. Guntherodt, Phys. Status Solidi A **202**, 754 (2005).

[2] R. Meijers, R. Calarco, N. Kaluza, H. Hardtdegen, M. V. D. Ahe, H. L. Bay, H. Luth, M. Buchmeier, and D. E. Burgler, J. Cryst. Growth **283**, 500 (2005).

[3] M. Buchmeier, D. E. Burgler, P. A. Grunberg, C. M. Schneider, R. Meijers, R. Calarco, C. Raeder, and M. Farle, Phys. Status Solidi A **203**, 1567 (2006).

[4] A. Navarro-Quezada, T. Li, C. Simbrunner, M. Kiecana, G. Hernandez-Sosa, M. Quast, M. Wegscheider, M. Sawicki, T. Dietl, and A. Bonanni, J. Cryst. Growth **310**, 1772 (2008).

[5] C. X. Gao, O. Brandt, H. P. Schonherr, U. Jahn, J. Herfort, and B. Jenichen, Appl. Phys. Lett. **95**, 111906 (2009).

[6] R. Gonzalez-Hernandez, W. Lopez, M. G. Moreno-Armenta, and J. A. Rodriguez, J. Appl. Phys. **109**, 07C102 (2011).

[7] R. Gonzalez-Hernandez, W. Lopez-Perez, M. G. Moreno-Armenta, and J. A. Rodriguez, J. Appl. Phys. **110**, 083712 (2011).

[8] L. Palomino-Rojas, R. Garcia-Diaz, G. H. Cocoletzi, and N. Takeuchi, J. Cryst. Growth **338**, 62 (2012).

[9] E. Lu, D. C. Ingram, A. R. Smith, J. W. Knepper, and F. Y. Yang, Phys. Rev. Lett. **97**, 146101 (2006).

[10] A. Bedoya-Pinto, C. Zube, J. Malindretos, A. Urban, and A. Rizzi, Phys. Rev. B **84**, 104424 (2011).

[11] K. Wang, E. Lu, J. W. Knepper, F.-Y. Yang, and A. R. Smith, Appl. Phys. Lett. **98**, 162507 (2011).

[12] J. Dumont, B. J. Kowalski, M. Pietrzyk, T. Seldrum, L. Houssiau, B. Douhard, I. Grzegory, S. Porowski, and R. Sporken, Superlattices Microstruct. **40**, 607 (2006).

[13] Y. Qi, G. F. Sun, M. Weinert, and L. Li, Phys. Rev. B **80**, 235323 (2009).

[14] K. Wang, N. Takeuchi, A. V. Chinchore, W. Lin, Y. Liu, and A. R. Smith, Phys. Rev. B **83**, 165407 (2011).

[15] A. R. Smith, R. M. Feenstra, D. W. Greve, J. Neugebauer, and J. E. Northrup, Phys. Rev. Lett. **79**, 3934 (1997).

[16] A. R. Smith, R. M. Feenstra, D. W. Greve, J. Neugebauer, and J. E. Northrup, Appl. Phys. A **66**, S947 (1998).

[17] A. R. Smith, V. Ramachandran, R. M. Feenstra, D. W. Greve, M.-S. Shin, M. Skowronski, J. Neugebauer, and J. E. Northrup, J. Vac. Sci. Technol. A **16**, 1641 (1998).

[18] Abhijit Chinchore, Kangkang Wang, Wenzhi Lin, and Arthur R. Smith, Appl. Phys. Lett. **93**, 181908 (2008).

[19] M. Shi, A. Chinchore, K. Wang, A.-O. Mandru, Y. Liu, and A. R. Smith, J. Appl. Phys. **112**, 053517 (2012).

[20] J. M. Soler, E. Artacho, J. D. Gale, A. Garcia, J. Junquera, P. Ordejón, and D. Sánchez-Portal, J. Phys.: Condens. Matter **14**, 2745 (2002).

[21] D. M. Ceperley and B. J. Alder, Phys. Rev. Lett. **45**, 566 (1980).

[22] J. P. Perdew and A. Zunger, Phys. Rev. B **23**, 5048 (1981).

[23] N. Troullier and J. L. Martins, Phys. Rev. B **43**, 1993 (1991).

[24] L. Kleinman and D. M. Bylander, Phys. Rev. Lett. **48**, 1425 (1982).

[25] S. G. Louie, S. Froyen, and M. L. Cohen, Phys. Rev. B **26**, 1738 (1982).

[26] H. A. H. AL-Brithen. R. Yang, M. B. Haider, C. Constantin, E. Lu, A. R. Smith, N. Sandler, and P. Ordejón, Phys. Rev. Lett. **95**, 146102 (2005).

[27] V. Ferrari, J. M. Pruneda, and E. Artacho, Phys. Status Solidi A **203**, 1437 (2006).

[28] J. Moreno and J. M. Soler, Phys. Rev. B **45**, 13891 (1992).

[29] Guo-Xin Qian, R. M. Martin, and D. J. Chadi, Phys. Rev. B **38**, 7649 (1988).

[30] P. H. T. Philipsen and E. J. Baerends, Phys. Rev. B **54**, 5326 (1996).

[31] X. Y. Cui, B. Delley, A. J. Freeman, and C. Stampfl, Phys. Rev. B **76**, 045201 (2007).

[32] J. Tersoff and D. R. Hamann, Phys. Rev. Lett. **50**, 1998 (1983).

[33] I. Horcas, R. Fernandez, J. M. Gomez-Rodriguez, J. Colchero, J. Gomez-Herrero, and A. M. Baro, Rev. Sci. Instrum. **78**, 013705 (2007).